Intratumorally Injected ^{177}Lu-Labeled Gold Nanoparticles: Gold Nanoseed Brachytherapy with Application for Neoadjuvant Treatment of Locally Advanced Breast Cancer

Simmyung Yook[1], Zhongli Cai[1], Yijie Lu[2], Mitchell A. Winnik[2], Jean-Philippe Pignol[3,4], and Raymond M. Reilly[1,5,6]

[1]Department of Pharmaceutical Sciences, University of Toronto, Toronto, Ontario, Canada; [2]Department of Chemistry, University of Toronto, Toronto, Ontario, Canada; [3]Department of Medical Biophysics, Toronto, Ontario, Canada; [4]Department of Radiation Oncology, Erasmus MC Cancer Institute, Rotterdam, The Netherlands; [5]Department of Medical Imaging, University of Toronto, Toronto, Ontario, Canada; and [6]Toronto General Research Institute, University Health Network, Toronto, Ontario, Canada

Improvements in the treatment of locally advanced breast cancer (LABC) are needed. Our objective was to study a radiation nanomedicine (gold nanoseeds) composed of 30-nm gold nanoparticles (AuNP) modified with polyethyleneglycol (PEG) chains linked to DOTA for complexing the β-particle emitter ^{177}Lu and to panitumumab for targeting epidermal growth factor receptors (EGFR) (^{177}Lu-T-AuNP) as a novel neoadjuvant brachytherapy for LABC. Nontargeted gold nanoseeds (^{177}Lu-NT-AuNP) were constructed without panitumumab for comparison. **Methods:** ^{177}Lu-T-AuNP or ^{177}Lu-NT-AuNP was injected intratumorally in CD-1 athymic mice bearing subcutaneous EGFR-positive MDA-MB-468 human breast cancer tumors. Biodistribution and small-animal SPECT/CT imaging studies were performed to evaluate tumor and normal organ localization. A short-term (15 d) study was conducted to select the most effective amount of ^{177}Lu-T-AuNP or ^{177}Lu-NT-AuNP for treatment with long-term observation (90–120 d). Normal organ toxicities were assessed by monitoring body weight, blood cell counts, and serum alanine aminotransferase and creatinine. Radiation-absorbed doses in the tumor and normal organs were estimated by Monte Carlo N-Particle version 5.0 modeling. **Results:** Tumor radioactivity concentrations were high at 1 h after injection (>300–400 percentage injected dose per gram [%ID/g]) but decreased by 2–3-fold at 48 h after injection. Normal organ uptake was low (<0.5 %ID/g) except for the liver and spleen (<3 %ID/g), increasing by 2–5-fold at 48 h after injection. Treatment with 4.5 MBq (6×10^{11} AuNP) of ^{177}Lu-T-AuNP or ^{177}Lu-NT-AuNP arrested tumor growth over 90 d without normal organ toxicity, whereas tumors continued to grow in mice treated with unlabeled T-AuNP or ^{177}Lu-labeled PEG polymer not linked to AuNP. Survival was prolonged up to 120 d in mice treated with ^{177}Lu-T-AuNP or ^{177}Lu-NT-AuNP. Radiation-absorbed doses to the tumor were 30 and 22 Gy for ^{177}Lu-T-AuNP and ^{177}Lu-NT-AuNP, respectively. Some tumor regions received high radiation doses (250–1,300 Gy). Normal organ doses were low (0.04–0.6 Gy). **Conclusion:** Gold nanoseeds injected intratumorally were highly effective for inhibiting the growth of breast cancer tumors in CD-1 athymic mice and caused no normal organ toxicity. These results are promising for their application for neoadjuvant brachytherapy of LABC. Because EGFR targeting was not required, the approach is broadly applicable to LABC with different phenotypes.

Received Oct. 26, 2015; revision accepted Jan. 21, 2016.

For correspondence or reprints contact: Raymond M. Reilly, Leslie Dan Faculty of Pharmacy, University of Toronto, 144 College St., Toronto, ON, Canada, M5S 3M2.

E-mail: raymond.reilly@utoronto.ca

Published online Feb. 4, 2016.

Key Words: gold nanoparticles; ^{177}Lu; epidermal growth factor receptor (EGFR); locally advanced breast cancer; brachytherapy

J Nucl Med 2016; 57:936–942
DOI: 10.2967/jnumed.115.168906

The systematic implementation of screening mammography for breast cancer (BC) has resulted in a downward stage migration, with most cases now diagnosed at an early stage, leading to a significant improvement in patient survival (*1–3*). However, locally advanced breast cancer (LABC) continues to represent about 5%–10% of newly diagnosed BC and is more frequent in emerging countries without screening programs (*4,5*). LABC carries a poor prognosis, with survival less than 50% at 5 y. One of the most important prognostic factors for LABC is the response to neoadjuvant chemotherapy, with overall survival reaching up to 80% at 5 y for patients who achieve a pathologic complete response (pCR) at the time of mastectomy (*6*). The mechanism by which pCR induced by neoadjuvant chemotherapy leads to better patient survival is not well understood. On the one hand, pCR may be considered as a surrogate of the chemosensitivity of distant micrometastasis (*7,8*). On the other hand, the Hellman theory predicts that better local control may prevent seeding or reseeding microscopic metastases between or after chemotherapy (*9*). Unfortunately, the pCR rate ranges from 3% to 27% (*10*), and none of the randomized trials evaluating more aggressive chemotherapy regimens have improved the survival of patients with LABC (*11,12*). Novel approaches, including radiotherapy, are needed to increase the pCR rate for LABC. Combined neoadjuvant chemoradiotherapy has been studied including neoadjuvant high-dose rate brachytherapy (BRT) (*13,14*), but these modalities are difficult to organize and deliver effectively in the neoadjuvant setting and notably in some cases have resulted in acute radiation–induced side effects (*15*).

We propose here a novel radiation nanomedicine BRT approach for neoadjuvant treatment of LABC (Fig. 1), which uses local intratumoral injection of 30-nm-diameter gold nanoparticles (AuNP) modified with polyethylene glycol (PEG) chains derivatized with DOTA that complex the radionuclide ^{177}Lu (half-life [$t_{1/2}$], 6.7 d) and with PEG chains linked to panitumumab (Vectibix; Amgen) that bind the AuNP to epidermal growth factor receptor (EGFR)–positive tumor cells (*16*). LABC is classified as triple-negative BC in one third of cases (*17*), and EGFR are overexpressed in 60% of

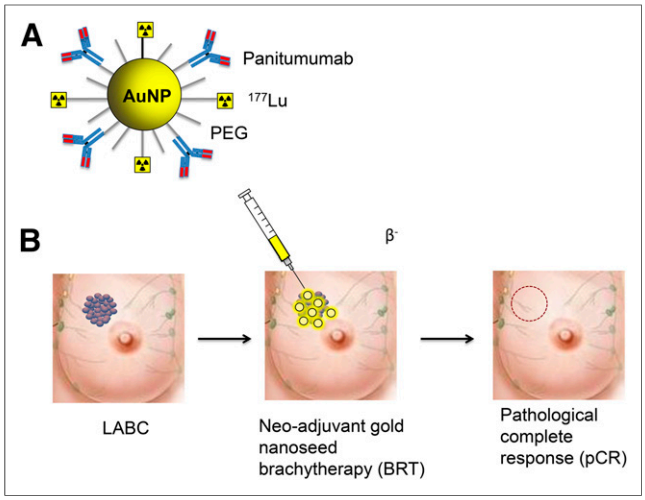

FIGURE 1. (A) Targeted gold nanoseeds composed of 30-nm-diameter AuNP modified with PEG chains linked to panitumumab and PEG chains linked to DOTA to complex ^{177}Lu. Nontargeted gold nanoseeds were not modified with panitumumab. (B) Radiation nanomedicine strategy for neoadjuvant BRT of LABC using gold nanoseeds injected intra- or peritumorally for radiation treatment of tumors. The aim is to increase the likelihood of pCR, which is predictive of better long-term outcome after surgical treatment. Adapted from © 2012 Terese Winslow LLC, U.S. Govt. has certain rights.

triple-negative BC (*18*). In an earlier study, we found that exposure of EGFR-positive MDA-MB-468 human BC cells in vitro to these EGFR-targeted AuNP (^{177}Lu-T-AuNP) dramatically decreased their clonogenic survival to less than 0.001%, whereas nontargeted ^{177}Lu-NT-AuNP diminished cell survival to 8.4% (*16*). Our aim in the current study was to investigate ^{177}Lu-NT-AuNP as a diffusable form of BRT seeds (i.e., gold nanoseeds) for local radiation treatment of BC, with particular application for neoadjuvant treatment of LABC.

There are several potential advantages of gold nanoseed BRT compared with conventional BRT seeds. First, because they are in a microscopically dispersed liquid form, they can be injected intra- or peritumorally by syringe and needle, which is less invasive than insertion of solid BRT seeds into the breast using catheters. Multiple small injections could be used to achieve a more homogeneous intra- or peritumoral distribution of the gold nanoseeds. Second, their nanometer size may permit local diffusion from the injection site, thus further homogenizing the radiation dose deposition in the tumor. Furthermore, because the moderate-energy β-particles emitted by ^{177}Lu ($E\beta_{max}$ = 0.50 MeV [78.6%], 0.38 MeV [9.1%], 0.18 MeV [12.2%]) have a 2-mm maximum range, this provides a conformal radiation field around the injection site and a local cross-fire effect. The cross-fire effect is expected to smoothen the dose deposition compared with the more heterogeneous distribution of gold nanoseeds in the tumor. The higher-energy (0.18–0.5 MeV) β-particles emitted by ^{177}Lu combined with a higher dose rate due to its shorter $t_{1/2}$ (6.7 d) may also be more effective for tumor treatment than low-energy γ-photons emitted by longer-lived ^{125}I (28 keV; $t_{1/2}$, 60 d) or ^{103}Pd (21 keV; $t_{1/2}$, 17 d) BRT seeds. Finally, the low-abundance γ-photons of ^{177}Lu ($E\gamma$ = 113 keV [3%] and 210 keV [11%]) enable SPECT imaging to assess the tumor and normal tissue distribution of the gold nanoseeds and estimate the tumor radiation dose deposition. ^{177}Lu-T-AuNP was more efficiently bound by EGFR-positive MDA-MB-468 cells than ^{177}Lu-NT-AuNP and was more cytotoxic in vitro (*16*), but it is not known if EGFR targeting would be required in vivo after intratumoral injection of gold nanoseeds due to their local tumor deposition. Therefore, we compared the effectiveness of EGFR-targeted and nontargeted gold nanoseeds for treatment of subcutaneous MDA-MB-468 tumors in CD-1 athymic mice. The radiation-absorbed doses to the tumor and normal tissues were estimated, and the normal tissue toxicity was also assessed.

MATERIALS AND METHODS

Cell Lines and Tumor Xenografts

MDA-MB-468 human BC cells (1×10^6 EGFR/cell; American Type Culture Collection) (*19*) were cultured at 37°C and 5% CO_2 in Dulbecco modified Eagle medium supplemented with 10% fetal bovine serum (Gibco-Invitrogen), penicillin (100 U/mL), streptomycin (100 μg/mL), 4 mM glutamine, and 400 μM sodium pyruvate. Tumor xenografts (diameter, 5–7 mm) were established in female CD-1 athymic mice (Charles River) by subcutaneous inoculation of 1×10^7 MBA-MB-468 cells in serum-free Dulbecco modified Eagle medium (100 μL) into the right flank. All animal studies were conducted in compliance with Canadian Council on Animal Care regulations and were performed under a protocol approved by the Animal Care Committee at the University Health Network (AUP 2780.1).

Construction and Characterization of Gold Nanoseeds

EGFR-targeted ^{177}Lu-labeled AuNP (^{177}Lu-T-AuNP) modified with panitumumab was constructed as previously reported by linking 30-nm-diameter (8% coefficient of variation) AuNP (Ted Pella) to orthopyridyl disulfide (OPSS)-PEG-DOTA (4 kDa) labeled with ^{177}Lu (PerkinElmer) and OPSS-PEG-panitumumab (5 kDa) (*16*). Nontargeted AuNP was not modified with panitumumab. OPSS-PEG-panitumumab was synthesized as previously reported (*16*) by reaction of panitumumab with OPSS-PEG-succinimidyl valerate (SVA) (5 kDa; Laysan Bio) containing a terminal SVA group. OPSS-PEG-DOTA (5 μg) was labeled by incubation with 3.0 MBq of $^{177}LuCl_3$ (PerkinElmer) in 0.1 M sodium acetate buffer, pH 6.0, at 80°C for 20 min. The synthesis and characterization of OPSS-PEG-DOTA were previously reported (*16*). OPSS-PEG-DOTA-^{177}Lu was purified on a polyacrylamide P6 mini-column (Bio-Gel P6; BioRad) eluted with ddH_2O (*16*). AuNP was stabilized by surface coating with a saturating amount of SH-PEG (2 kDa; Laysan Bio). Radiolabeled AuNP were purified by ultracentrifugation, and the final specific activity was 1.5 MBq/2.0×10^{11} AuNP.

Biodistribution and Small-Animal SPECT/CT Imaging Studies

Biodistribution studies were performed in groups of 4–8 female CD-1 athymic mice bearing subcutaneous MDA-MB-468 xenografts after intratumoral injection using an Ultra-fine 1-cc insulin syringe (U-100 with attached 29G1/2″ needle; Becton Dickinson) over 5 min of 1–2 MBq (6×10^{11} AuNP) of ^{177}Lu-T-AuNP or ^{177}Lu-NT-AuNP suspended in 30 μL of normal saline. At 1 or 48 h after injection, the mice were sacrificed and the tumor and samples of normal tissues including blood were collected. The radioactivity in each was measured in a γ-counter (Wizard Model 1480; PerkinElmer) and expressed as percentage injected dose per gram (%ID/g). Small-animal SPECT/CT imaging was performed on groups of 3–4 mice with subcutaneous MDA-MB-468 xenografts at 1, 6, 24, and 48 h after intratumoral injection of 4–5 MBq (6×10^{11} AuNP) of ^{177}Lu-T-AuNP or ^{177}Lu-NT-AuNP. Images were acquired on a nanoSPECT/CT tomograph (Bioscan) equipped with 4 sodium iodide (NaI) detectors and fitted with 1.4-mm multipinhole collimators (full width at half maximum height, 1.2 mm). Mice were anesthetized by inhalation of 2% isoflurane in O_2, and body temperature was maintained at 37°C using a Minerve bed (Bioscan). At each time point, 82 SPECT projections were acquired in a 124 × 124 × 1 (37.2 × 37.2 × 0.3 mm)

voxel acquisition matrix corresponding to a resolution of 0.3 mm/pixel. Images were acquired for 150, 154, 166, and 184 s/projection at 1, 6, 24, and 48 h after injection, respectively, to account for decay of ^{177}Lu. Images were reconstructed using an ordered-subset expectation maximization algorithm (9 iterations). Cone-beam CT images were acquired (126 projections, 1 s/projection, 45 kVp) in a 176 × 176 × 1 (37.2 × 37.2 × 0.21 mm) voxel acquisition matrix (0.21 mm/pixel). Small-animal SPECT and CT images were coregistered using InvivoScope software (Bioscan). Volume-of-interest analysis of the images was performed using Image J software (U.S. National Institutes of Health). Details of the Image J analysis of the small-animal SPECT images are provided in the supplemental materials (available at http://jnm.snmjournals.org).

Radiation-Absorbed Dose Estimates

The %ID/organ values for normal tissues were calculated by multiplying the %ID/g from biodistribution studies by standard organ weights for mice (*20*). Similarly, the %ID in the tumor was calculated by multiplying the weight of the tumor (g) by the %ID/g. Assuming an injected dose of 4.5 MBq, the tumor or normal organ radioactivity at 1 or 48 h was calculated. Cumulative radioactivity ($\tilde{A}_{0-48h}$) not corrected for radioactive decay was estimated for the tumor and normal organs from the area under the curve from 0 to 48 h (Bq × second [s]) calculated using the trapezoidal rule (*21*). The combined $\tilde{A}_{0-48h}$ values for each organ were multiplied by the S value (Gy/Bq × s) for ^{177}Lu to estimate the radiation-absorbed doses (Gy) up to 48 h after injection for intratumoral injection of 4.5 MBq of ^{177}Lu-T-AuNP or ^{177}Lu-NT-AuNP. The S values for mouse organs were taken from Bitar et al. (*20*), whereas the S value for the tumor was calculated by Monte Carlo N-Particle (version 5.0; Los Alamos Laboratory) modeling assuming a 6-mm-diameter sphere in which ^{177}Lu was distributed homogeneously. The submillimeter voxel (0.3 × 0.3 × 0.3 mm^3)–based S values of ^{177}Lu were calculated using Monte Carlo N-Particle, and the radioactivity in each voxel was derived from small-animal SPECT images using ImageJ and MATLAB R2014b (MathWorks). MATLAB was also used to calculate the cumulative radioactivities and radiation-absorbed doses in each voxel and to plot the tumor dose map by displaying isoradioactivity and isodose contours. Details of the radiation dosimetry calculations are provided in the supplemental materials.

Dose Selection and Normal Organ Toxicity Study

A short-term (15 d) study was conducted to select the amount of ^{177}Lu-T-AuNP for administration in a long-term observation (90–120 d) treatment study (supplemental materials). Briefly, groups of 3–5 CD-1 athymic mice with subcutaneous MDA-MB-468 tumors were injected intratumorally with 0.3–4.5 MBq of ^{177}Lu-T-AuNP (2–6 × 10^{11} AuNP) or with unlabeled-T-AuNP or normal saline. Tumor volume was measured, and a tumor growth index (TGI) was calculated by dividing the tumor volume at each time point by the initial tumor volume before treatment. Similarly, a body weight index (BWI) was calculated by dividing the body weight at each time point by the initial body weight. The mean TGI and BWI were plotted versus the time after treatment. At 15 d, a complete blood cell count was obtained, and serum alanine aminotransferase (ALT) and creatinine were measured as described in the supplemental materials.

Long-Term Treatment Study

Groups of 6–7 mice with subcutaneous MDA-MB-468 tumor xenografts were injected intratumorally with 4.5 MBq (6 × 10^{11} particles) of ^{177}Lu-T-AuNP or ^{177}Lu-NT-AuNP in 30 μL of normal saline as described earlier. Control groups of mice were injected intratumorally with unlabeled T-AuNP or normal saline or received an intratumoral injection of 4.5 MBq (7.5 μg) of unconjugated OPSS-PEG-DOTA-^{177}Lu. Mice were monitored for tumor growth for 90 d or until tumor size reached 12 mm (the humane endpoint of the animal care protocol) and were sacrificed. Tumor volume was independently measured by 2 observers using digital calipers (VWR) twice a week for 30 d and once a week for the following 60 d as detailed in the methods for the dose-selection study in the supplemental materials. Body weight was monitored as described earlier, and the TGI and BWI were calculated. The study was extended to 120 d by continuing to monitor the survival of mice that had not reached the humane tumor size endpoint. Kaplan–Meier plots were constructed by plotting the proportion of mice sacrificed versus the time after treatment. The median survival for each group was calculated.

Statistical Analysis

Results were expressed as mean ± SD and tested for statistical significance using a 2-sided Student *t* test. The level of significance was set at a *P* value of less than 0.05.

RESULTS

Construction and Characterization of Gold Nanoseeds

Gold nanoseeds (Fig. 1) were constructed and characterized as previously reported (*16*). The mean hydrodynamic diameter of unmodified AuNP determined by dynamic light scattering was 36.7 ± 0.2 nm, whereas the corresponding sizes of unlabeled T-AuNP and NT-AuNP were 67.3 ± 0.6 and 45.8 ± 0.6 nm, respectively. The surface charge of unmodified AuNP was −48.5 ± 1.5 mV, whereas the surface charges of unlabeled NT-AuNP and unlabeled T-AuNP were −53.4 ± 2.0 and −48.8 ± 1.0 mV, respectively.

Biodistribution and Small-Animal SPECT/CT Imaging Studies

Biodistribution studies revealed that intratumoral injection of ^{177}Lu-T-AuNP and ^{177}Lu-NT-AuNP resulted in high tumor concentrations of radioactivity at 1 h after injection (Fig. 2). There was no significant difference in tumor radioactivity at this time

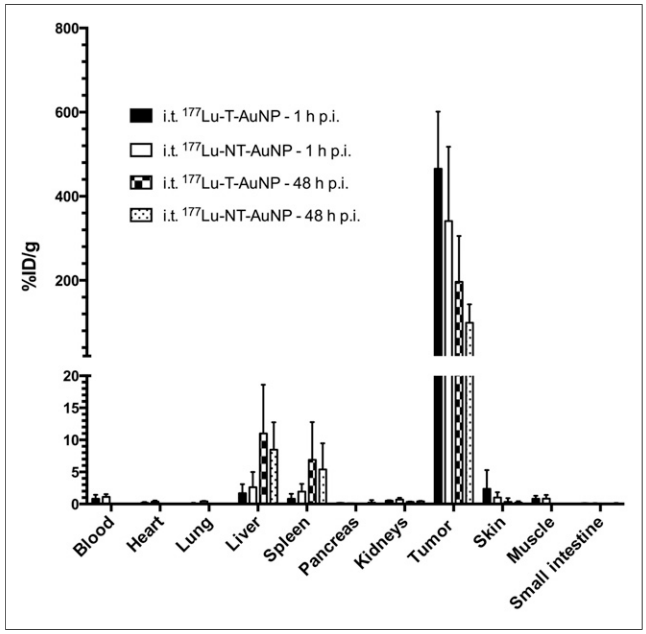

FIGURE 2. Tumor and normaltissue biodistribution of ^{177}Lu-T-AuNP and ^{177}Lu-NT-AuNP at 1 or 48 h after intratumoral (i.t.) injection in CD-1 athymic mice with subcutaneous MDA-MB-468 human BC xenografts. Values shown represent mean ± SD (n = 4–8). p.i. = after injection.

point for ^{177}Lu-T-AuNP or ^{177}Lu-NT-AuNP (465.7 ± 135.6 vs. 341.1 ± 176.6 %ID/g; $P = 0.36$). Tumor radioactivity decreased from 1 to 48 h after injection for ^{177}Lu-T-AuNP and ^{177}Lu-NT-AuNP, but there was 2-fold-greater retention of ^{177}Lu-T-AuNP than ^{177}Lu-NT-AuNP at 48 h after injection (196.6 ± 109.2 vs. 99.0 ± 44.0 %ID/g; $P = 0.05$). Liver radioactivity was low at 1 h after injection for ^{177}Lu-T-AuNP and ^{177}Lu-NT-AuNP (1.7 ± 1.4 and 2.6 ± 2.4 %ID/g, respectively; $P = 0.57$) but increased by 6.5- and 3.3-fold, respectively, at 48 h after injection (11.0 ± 7.6 and 8.5 ± 4.3 %ID/g, respectively). Similarly, spleen radioactivity was low at 1 h after injection for ^{177}Lu-T-AuNP and ^{177}Lu-NT-AuNP (0.8 ± 0.8 and 1.9 ± 1.2 %ID/g, respectively) but increased by 8.6- and 2.8-fold to 6.9 ± 5.9 and 5.4 ± 4.1 %ID/g at 48 h after injection. There were no significant differences in the liver and spleen uptake at 48 h after injection for ^{177}Lu-T-AuNP or ^{177}Lu-NT-AuNP. Radioactivity in all other organs was less than 0.5 %ID/g at 1 or 48 h after injection.

Small-animal SPECT/CT images revealed radioactivity mostly confined to the subcutaneous MDA-MB-468 tumors at 1 h after intratumoral injection of ^{177}Lu-T-AuNP or ^{177}Lu-NT-AuNP (Fig. 3A), but there was a decrease in tumor radioactivity at 48 h after injection. Tumor radioactivity appeared more homogeneous at 48 h after injection, suggesting intratumoral diffusion of the radiolabeled AuNP. Volume-of-interest analysis of the images acquired at 1, 6, 24, and 48 h after injection (Fig. 3B) showed a similar rate of elimination of tumor radioactivity for mice injected with ^{177}Lu-T-AuNP or ^{177}Lu-NT-AuNP.

Radiation Dosimetry Estimates

Radiation doses deposited in the tumor were high but were not significantly different for ^{177}Lu-T-AuNP and ^{177}Lu-NT-AuNP (30.4 ± 10.4 vs. 21.9 ± 11.6 Gy, respectively; $P = 0.30$; Table 1). The radiation doses deposited in normal organs were 33–760-fold lower for ^{177}Lu-T-AuNP and 27–364-fold lower for ^{177}Lu-NT-AuNP than the tumor dose (Table 1). The highest normal organ doses were received by the liver, spleen, and pancreas. The total-body radiation dose was 0.35 and 0.44 Gy for ^{177}Lu-T-AuNP and ^{177}Lu-NT-ANP, respectively. Figure 4 shows the regional distribution of radiation dose and radioactivity in a tumor from a representative mouse injected with gold nanoseeds in 1 plane (6.3 × 6.3 mm) perpendicular to the line of injection of ^{177}Lu-T-AuNP and ^{177}Lu-NT-AuNP at 48 h after injection. In this plane, the isodose contours ranged from 0 to 1,300 Gy and from 0 to 250 Gy for ^{177}Lu-T-AuNP and ^{177}Lu-NT-AuNP, respectively, whereas the isoradioactivity contours for ^{177}Lu-T-AuNP and ^{177}Lu-NT-AuNP ranged from 0 to 2,750 Bq and from 0 to 400 Bq, respectively.

TABLE 1
Radiation-Absorbed Doses to Tumor and Normal Organs in CD-1 Athymic Mice with Subcutaneous MDA-MB-468 Human BC Xenografts Injected Intratumorally with 4.5 MBq of ^{177}Lu-T-AuNP or ^{177}Lu-NT-AuNP

Organ	Radiation-absorbed dose (Gy)*	
	^{177}Lu-T-AuNP	^{177}Lu-NT-AuNP
Heart	0.04 ± 0.03	0.06 ± 0.04
Lungs	0.13 ± 0.11	0.15 ± 0.12
Liver	0.91 ± 0.63	0.82 ± 0.49
Spleen	0.64 ± 0.48	0.55 ± 0.40
Pancreas	0.31 ± 0.13	0.25 ± 0.16
Kidneys	0.11 ± 0.03	0.12 ± 0.05
Intestine	0.06 ± 0.04	0.06 ± 0.04
Tumor	30.37 ± 10.36	21.86 ± 11.64
Total body	0.35 ± 0.35	0.44 ± 0.39

*Cumulative radiation-absorbed dose from 0 h after injection to 48 h after injection of ^{177}Lu-T-AuNP or ^{177}Lu-NT-AuNP based on biodistribution data shown in Figure 2. Values represent mean ± SD (n = 4–8).

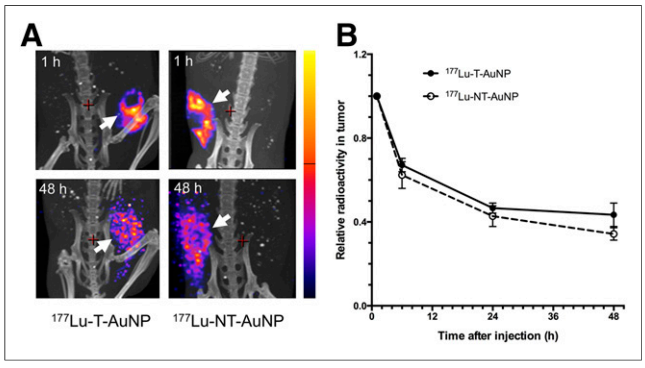

FIGURE 3. (A) Posterior small-animal SPECT/CT images of pelvis of representative CD-1 athymic mice with subcutaneous MDA-MB-468 human BC xenografts (white arrows) at 1 or 48 h after intratumoral injection of ^{177}Lu-T-AuNP or ^{177}Lu-NT-AuNP. Intensity bar on right represents range of intensities (arbitrary units) for all panels, which have been normalized to same intensity scale. (B) Relative tumor radioactivity in tumor-bearing mice at different times after intratumoral injection of ^{177}Lu-T-AuNP or ^{177}Lu-NT-AuNP determined by volume-of-interest analysis of the images. Values shown represent mean ± SD (n = 3–4).

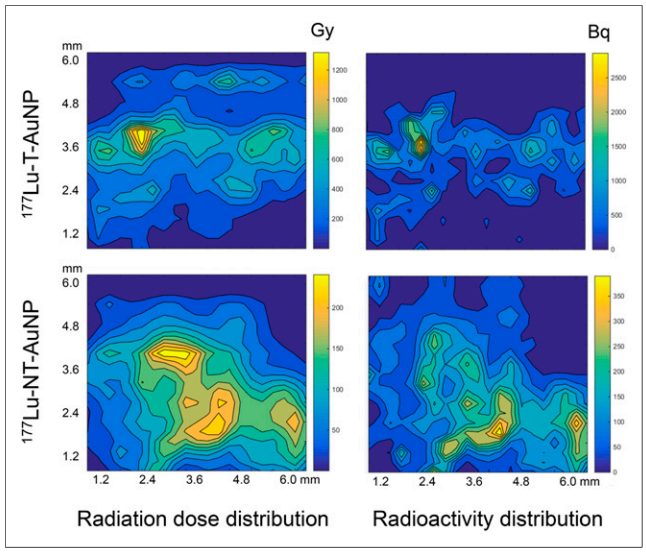

FIGURE 4. Comparison of radiation-absorbed dose distribution (left) and radioactivity distribution (right) in representative subcutaneous MDA-MB-468 human BC xenograft in CD-1 athymic mouse at 48 h after intratumoral injection of ^{177}Lu-T-AuNP (top) or ^{177}Lu-NT-AuNP (bottom).

Dose Selection and Normal Organ Toxicity Study

The effects of intratumoral injection of ^{177}Lu-T-AuNP on the TGI and BWI in CD-1 athymic mice bearing subcutaneous MDA-MB-468 tumor xenografts over a 15-d period are shown in Supplemental Fig. 1. On the basis of the results of these studies, a dose of 4.5 MBq (6×10^{11} AuNP) of ^{177}Lu-T-AuNP was selected for treatment with long-term (90–120 d) observation. At this administered amount of ^{177}Lu-T-AuNP, the TGI was 32.2-fold ($P < 0.001$) significantly lower than for mice treated with normal saline and 38.4-fold ($P < 0.001$) lower than for mice treated with unlabeled T-AuNP (Supplemental Fig. 1A). There was no significant effect in the BWI for mice treated with unlabeled T-AuNP or normal saline (Supplemental Fig. 1B). There was also no significant decrease in blood cell counts or increased ALT or serum creatinine for mice injected with ^{177}Lu-T-AuNP compared with mice receiving unlabeled T-AuNP or normal saline (Table 2). The supplemental materials provide a detailed description of the results of these dose-selection studies.

Long-Term Treatment Study

^{177}Lu-T-AuNP or ^{177}Lu-NT-AuNP (4.5 MBq; 6×10^{11} AuNP) arrested the growth of subcutaneous MDA-MB-468 xenografts in CD-1 athymic mice, whereas unlabeled T-AuNP, OPSS-PEG-DOTA-^{177}Lu, or normal saline was not effective (Fig. 5A). The mean TGI at 90 d in mice injected with ^{177}Lu-T-AuNP (0.3 ± 0.3) was 35.1-fold significantly lower than for mice receiving normal saline (11.1 ± 7.6; $P = 0.005$) and 30.0-fold lower than for mice injected with unlabeled-T-AuNP (9.5 ± 1.8; $P < 0.001$). No significant differences in TGI were found between mice treated with ^{177}Lu-T-AuNP or ^{177}Lu-NT-AuNP (TGI = 0.3 ± 0.3 vs. 0.8 ± 0.9, respectively; $P = 0.19$). Kaplan–Meier survival curves (Fig. 5C) revealed that all mice treated with ^{177}Lu-T-AuNP or ^{177}Lu-NT-AuNP survived until 120 d, whereas the median survival of mice injected with unlabeled T-AuNP, unconjugated OPSS-PEG-DOTA-^{177}Lu polymer, or normal saline was 86, 82, and 75 d, respectively. Complete tumor regression, that is, absence of a measurable tumor volume at 120 d, was found in 3 of 6 mice treated with ^{177}Lu-T-AuNP and in 1 of 6 mice injected with ^{177}Lu-NT-AuNP. There were no significant differences in BWI over a 90-d period for mice receiving ^{177}Lu-T-AuNP, ^{177}Lu-NT-AuNP, unlabeled T-AuNP, OPSS-PEG-DOTA-^{177}Lu, or normal saline (Fig. 5B), and mice in all groups gained weight.

DISCUSSION

We report here the effectiveness and toxicity of a novel BRT approach to local radiation treatment of BC using intratumorally injected ^{177}Lu-labeled gold nanoseeds. There have been only a few other studies that have examined ^{177}Lu-labeled AuNP for tumor treatment. In one study, AuNP were modified with cyclic arginine-glycine-aspartate peptides to target $\alpha_v\beta_3$ integrins for treatment of glioma (*22*). In another study, bombesin peptide–modified ^{177}Lu-AuNP were investigated for combined photothermal and radiation therapy of prostate cancer (*23*). To our knowledge, our report is the first to study ^{177}Lu-AuNP for local treatment of BC. We hypothesized that targeting ^{177}Lu-T-AuNP to EGFR-positive BC cells would provide greater tumor retention and effectiveness than nontargeted ^{177}Lu-NT-AuNP after intratumoral injection. However, small-animal SPECT/CT imaging and biodistribution studies revealed that both forms of gold nanoseeds achieved high initial concentrations of radioactivity in MDA-MB-468 tumors (>300–400 %ID/g) at 1 h after intratumoral injection and were only slowly cleared over 48 h (Figs. 2 and 3). Consequently, both ^{177}Lu-T-AuNP and ^{177}Lu-NT-AuNP deposited high radiation doses (30 and 22 Gy, respectively) in tumors that were equivalently effective for arresting tumor growth (Fig. 5). The slow elimination of gold nanoseeds from the tumors was due to the properties of AuNP, which result in tumor retention after intratumoral injection (*24*). We previously found that ^{111}In-labeled AuNP modified with trastuzumab to target human epidermal growth factor receptor 2 was similarly retained by MDA-MB-361 human BC xenografts in mice after intratumoral injection, whereas intravenously injected AuNP were sequestered by the liver, spleen, and kidneys, greatly diminishing their tumor localization (*24*). OPSS-PEG-DOTA-^{177}Lu polymer not linked to AuNP injected intratumorally was ineffective for preventing tumor growth (Fig. 5), likely due to its poor tumor retention. Similar results were reported by Xie et al. for intratumorally injected nontargeted ^{64}Cu-labeled gold nanoshells, which were retained in head and neck squamous cell carcinoma xenografts in nude rats, whereas ^{64}Cu-DOTA or ^{64}Cu-DOTA-PEG not linked to the gold nanoshells were cleared from these tumors over 44 h (*25*). Liver and spleen uptake remains a major challenge to the use of systemically administered AuNP for cancer treatment (*26*), but this obstacle was overcome using intratumorally injected ^{177}Lu-T-AuNP and ^{177}Lu-NT-AuNP.

The high concentrations of radioactivity in MDA-MB-468 xenografts after intratumoral injection of ^{177}Lu-T-AuNP and ^{177}Lu-NT-AuNP (>300–400 %ID/g) resulted in high tumor radiation doses

TABLE 2
Hematology and Serum Biochemistry in CD-1 Athymic Mice with Subcutaneous MDA-MB-468 Human BC Xenografts at 15 Days After Intratumoral Injection of ^{177}Lu-T-AuNP, Unlabeled T-AuNP, or Normal Saline

Parameter	Normal saline	Unlabeled T-AuNP	^{177}Lu-T-AuNP (0.3 MBq)	^{177}Lu-T-AuNP (1.5 MBq)	^{177}Lu-T-AuNP (4.5 MBq)
White blood cells ($\times 10^9$/L)	5.9 ± 2.9	7.0 ± 3.3	5.3 ± 2.7	5.4 ± 3.2	4.9 ± 1.6
Red blood cells ($\times 10^{12}$/L)	9.1 ± 0.8	9.3 ± 0.5	8.0 ± 1.0	10.0 ± 0.9	9.9 ± 0.7
Hemoglobin (g/L)	13.7 ± 1.1	13.8 ± 0.4	12.2 ± 0.6	14.5 ± 0.8	14.6 ± 1.0
Hematocrit (%)	43.0 ± 3.7	44.5 ± 2.1	39.1 ± 2.7	47.9 ± 3.9	47.7 ± 3.5
ALT (U/L)	33.5 ± 19.3	18.8 ± 3.9	21.4 ± 0.6	25.5 ± 17.3	17.8 ± 8.6
Serum creatinine (μmol/L)	15.4 ± 5.7	16.1 ± 8.0	27.4 ± 26.9	22.1 ± 10.6	18.2 ± 7.0

Values represent mean ± SD (n = 3–6).

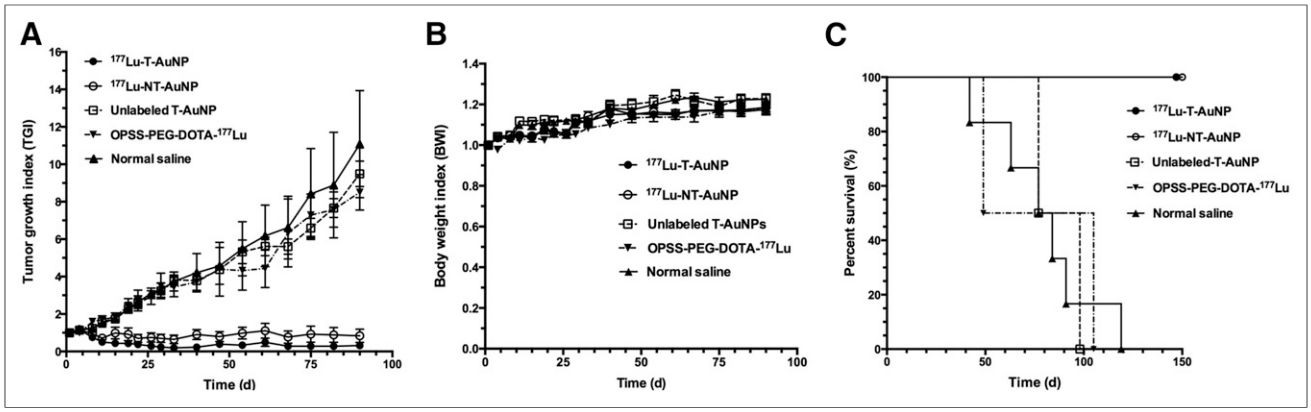

FIGURE 5. TGI (A), BWI (B), and percentage survival (C) vs. time for CD-1 athymic mice with subcutaneous MDA-MB-468 human BC xenografts treated with 4.5 MBq (6×10^{11} AuNP) of ^{177}Lu-T-AuNP, ^{177}Lu-NT-AuNP, or unlabeled T-AuNP or receiving OPSS-PEG-DOTA-^{177}Lu (not conjugated to AuNP) or normal saline. In A and B, values shown represent mean ± SD (n = 6–7).

(22–30 Gy; Table 1). Furthermore, mapping of the intratumoral dose distribution (Fig. 4, left) revealed that some regions received high doses (250–1,300 Gy). Notably, the isoradiation dose contours were smoothened and extended compared with the isoradioactivity contours (Fig. 4, right) due to the cross-fire effect from the 2-mm-range β-particles emitted by ^{177}Lu. The dose delivered to the tumor after a single intratumoral injection of ^{177}Lu-T-AuNP (30 Gy) or ^{177}Lu-NT-AuNP (22 Gy) was comparable to that prescribed for BC patients with conventional BRT (34–90 Gy) (*27*). Vilchis-Juárez et al. similarly reported tumor doses as high as 64 Gy after intratumoral injection of ^{177}Lu-labeled AuNP in mice with C6 glioma xenografts (*22*). The slow redistribution of ^{177}Lu-T-AuNP and ^{177}Lu-NT-AuNP over 48 h to normal tissues (<7–12 %ID/g) limited normal organ radiation doses to 0.04–0.6 Gy. There are currently no examples of intratumorally injected therapeutic radiopharmaceuticals, but the total-body dose for ^{177}Lu-DOTATATE, a radiopeptide administered intravenously for treatment of neuroendocrine tumors, is 0.05 mGy/MBq (*28*). On the basis of an administered amount of 2,500–7,500 MBq of ^{177}Lu-DOTATATE in humans, the total body radiation dose would be 0.12–0.37 Gy. This is comparable to the total-body dose estimated in mice for intratumorally injected ^{177}Lu-T-AuNP (0.35 Gy) or ^{177}Lu-NT-AuNP (0.44 Gy).

Tumor growth inhibition was directly dependent on the administered amount of ^{177}Lu-T-AuNP (0.3–4.5 MBq [$2–6 \times 10^{11}$ AuNP] in a short-term observation [15 d] study [Supplemental Fig. 1]), but no normal tissue toxicity was found at any amount. There were no significant decreases in red blood cells, white blood cells, hemoglobin, or hematocrit or increases in serum ALT or creatinine at 15 d, compared with mice receiving unlabeled AuNP or normal saline (Table 2). The absence of normal tissue toxicity was confirmed in a long-term treatment study. Mice maintained or increased their body weight over 90 d when treated with 4.5 MBq (6×10^{11} AuNP) of ^{177}Lu-T-AuNP or ^{177}Lu-NT-AuNP (Fig. 5C). This injected amount of both forms of gold nanoseeds was highly effective for arresting tumor growth, and no regrowth was detected up to 90 d (Fig. 5A). In contrast, mice treated with unlabeled T-AuNP, unconjugated OPSS-PEG-DOTA-^{177}Lu, or normal saline exhibited rapid tumor growth. Furthermore, both ^{177}Lu-T-AuNP and ^{177}Lu-NT-AuNP treatment prolonged survival up to 120 d (Fig. 5B). Vilchis-Juárez et al. found that ^{177}Lu-AuNP targeted to $\alpha_v\beta_3$ integrins on C6 glioma xenografts were 3-fold more effective than nontargeted ^{177}Lu-AuNP for inhibiting tumor growth in contrast to the findings in our study (*22*). However, they similarly found that ^{177}Lu-cyclic arginine-glycine-aspartic acid peptides not linked to AuNP were 12-fold less effective than targeted ^{177}Lu-AuNP. Because we previously found that EGFR-targeted ^{177}Lu-T-AuNP was more potent in vitro than nontargeted ^{177}Lu-NT-AuNP for killing MDA-MB-468 cells (*16*), our results suggest that the intratumoral route of administration was responsible for the equivalent effectiveness in vivo of these 2 forms of the gold nanoseeds. The absence of normal tissue toxicity of the gold nanoseeds suggests that this form of BRT could be combined with neoadjuvant chemotherapy for treatment of LABC without increasing toxicity with the aim to improve the rate of pCR and achieve better patient outcomes. Clinical trials comparing this combination BRT and chemotherapy strategy with neoadjuvant chemotherapy alone will be required to determine whether there is an improvement in the pCR rate and in patient outcome.

CONCLUSION

Intratumorally injected ^{177}Lu-T-AuNP or ^{177}Lu-NT-AuNP arrested the growth of MDA-MB-468 human BC tumors in CD-1 athymic mice with no observable normal tissue toxicity. Because EGFR targeting did not provide greater tumor retention or higher tumor radiation-absorbed doses, and both ^{177}Lu-T-AuNP and ^{177}Lu-NT-AuNP were equivalently effective for arresting tumor growth, nontargeted gold nanoseeds could be applied for neoadjuvant BRT of LABC, which would broaden the approach to tumors expressing many different phenotypes.

DISCLOSURE

The costs of publication of this article were defrayed in part by the payment of page charges. Therefore, and solely to indicate this fact, this article is hereby marked "advertisement" in accordance with 18 USC section 1734. This research was supported by a grant from the Canadian Breast Cancer Foundation (Ontario Region) and a grant from the Natural Sciences and Engineering Research Council as well as an Ontario Graduate Scholarship (OGS), a scholarship from the Terry Fox Foundation Excellence in Radiation Research for the 21st Century Program, and a Pharmaceutical Sciences Graduate Student Association Fellowship to Simmyung Yook. No other potential conflict of interest relevant to this article was reported.

ACKNOWLEDGMENTS

Parts of this research were presented at the European Association of Nuclear Medicine Congress in Gothenburg, Sweden, October 18–22, 2014 (Eckert & Ziegler Young Investigator Award).

REFERENCES

1. Peto R, Boreham J, Clarke M, Davies C, Beral V. UK and USA breast cancer deaths down 25% in year 2000 at ages 20-69 years. *Lancet.* 2000;355:1822.
2. Nyström L, Andersson I, Bjurstam N, Frisell J, Nordenskjold B, Rutqvist LE. Long-term effects of mammography screening: updated overview of the Swedish randomised trials. *Lancet.* 2002;359:909–919.
3. Early Breast Cancer Trialists' Collaborative GroupDarby S, McGale P, et al. Effect of radiotherapy after breast-conserving surgery on 10-year recurrence and 15-year breast cancer death: meta-analysis of individual patient data for 10,801 women in 17 randomised trials. *Lancet.* 2011;378:1707–1716.
4. Apffelstaedt JP. Locally advanced breast cancer in developing countries: the place of surgery. *World J Surg.* 2003;27:917–920.
5. Yalcin B. Overview on locally advanced breast cancer: defining, epidemiology, and overview on neoadjuvant therapy. *Exp Oncol.* 2013;35:250–252.
6. Ferrière JP, Assier I, Cure H, et al. Primary chemotherapy in breast cancer: correlation between tumor response and patient outcome. *Am J Clin Oncol.* 1998;21: 117–120.
7. von Minckwitz G, Loibl S, Maisch A, Untch M. Lessons from the neoadjuvant setting on how best to choose adjuvant therapies. *Breast.* 2011;20(suppl 3):S142–S145.
8. Hanrahan EO, Hennessy BT, Valero V. Neoadjuvant systemic therapy for breast cancer: an overview and review of recent clinical trials. *Expert Opin Pharmacother.* 2005;6:1477–1491.
9. Hellman S. Stopping metastases at their source. *N Engl J Med.* 1997;337:996–997.
10. Mandilaras V, Bouganim N, Spayne J, et al. Concurrent chemoradiotherapy for locally advanced breast cancer-time for a new paradigm? *Curr Oncol.* 2015;22: 25–32.
11. Therasse P, Mauriac L, Welnicka-Jaskiewicz M, et al. Final results of a randomized phase III trial comparing cyclophosphamide, epirubicin, and fluorouracil with a dose-intensified epirubicin and cyclophosphamide + filgrastim as neoadjuvant treatment in locally advanced breast cancer: an EORTC-NCIC-SAKK multicenter study. *J Clin Oncol.* 2003;21:843–850.
12. Ellis GK, Barlow WE, Gralow JR, et al. Phase III comparison of standard doxorubicin and cyclophosphamide versus weekly doxorubicin and daily oral cyclophosphamide plus granulocyte colony-stimulating factor as neoadjuvant therapy for inflammatory and locally advanced breast cancer: SWOG 0012. *J Clin Oncol.* 2011;29:1014–1021.
13. Adams S, Chakravarthy AB, Donach M, et al. Preoperative concurrent paclitaxel-radiation in locally advanced breast cancer: pathologic response correlates with five-year overall survival. *Breast Cancer Res Treat.* 2010;124:723–732.
14. Roddiger SJ, Kolotas C, Filipowicz I, et al. Neoadjuvant interstitial high-dose-rate (HDR) brachytherapy combined with systemic chemotherapy in patients with breast cancer. *Strahlenther Onkol.* 2006;182:22–29.
15. Chow TL, Louie AV, Palma DA, et al. Radiation-induced lung injury after concurrent neoadjuvant chemoradiotherapy for locally advanced breast cancer. *Acta Oncol.* 2014;53:697–701.
16. Yook S, Cai Z, Lu Y, Winnik MA, Pignol JP, Reilly RM. Radiation nanomedicine for EGFR-positive breast cancer: panitumumab-modified gold nanoparticles complexed to the β-particle-emitter, ^{177}Lu. *Mol Pharm.* 2015;12:3963–3972.
17. Meyers MO, Klauber-Demore N, Ollila DW, et al. Impact of breast cancer molecular subtypes on locoregional recurrence in patients treated with neoadjuvant chemotherapy for locally advanced breast cancer. *Ann Surg Oncol.* 2011;18: 2851–2857.
18. Burness ML, Grushko TA, Olopade O. Epidermal growth factor receptor in triple-negative and basal-like breast cancer: promising clinical target or only a marker? *Cancer J.* 2010;16:23–32.
19. Reilly RM, Gariépy J. Factors influencing the sensitivity of tumor imaging with a receptor-binding radiopharmaceutical. *J Nucl Med.* 1998;39:1036–1043.
20. Bitar A, Lisbona A, Thedrez P, et al. A voxel-based mouse for internal dose calculations using Monte Carlo simulations (MCNP). *Phys Med Biol.* 2007;52: 1013–1025.
21. Appendix D. Estimation of Areas. In: Gibaldi M, Perrier D, eds. *Pharmacokinetics.* 2nd ed. New York, NY: Marcel Dekker Inc.; 1982: 445–449.
22. Vilchis-Juárez Vilchis-Juarez A, Ferro-Flores G, Santos-Cuevas C, et al. Molecular targeting radiotherapy with cyclo-RGDFK(C) peptides conjugated to ^{177}Lu-labeled gold nanoparticles in tumor-bearing mice. *J Biomed Nanotechnol.* 2014;10:393–404.
23. Jiménez-Mancilla N, Ferro-Flores G, Santos-Cuevas C, et al. Multifunctional targeted therapy system based on ^{99m}Tc/^{177}Lu-labeled gold nanoparticles-Tat(49-57)-Lys(3)-bombesin internalized in nuclei of prostate cancer cells. *J Labelled Comp Radiopharm.* 2013;56:663–671.
24. Chattopadhyay N, Fonge H, Cai Z, et al. Role of antibody-mediated tumor targeting and route of administration in nanoparticle tumor accumulation in vivo. *Mol Pharm.* 2012;9:2168–2179.
25. Xie H, Goins B, Bao A, Wang ZJ, Phillips WT. Effect of intratumoral administration on biodistribution of ^{64}Cu-labeled nanoshells. *Int J Nanomedicine.* 2012;7: 2227–2238.
26. Lee J, Chatterjee DK, Lee MH, Krishnan S. Gold nanoparticles in breast cancer treatment: promise and potential pitfalls. *Cancer Lett.* 2014;347:46–53.
27. Hepel JT, Wazer DE. A comparison of brachytherapy techniques for partial breast irradiation. *Brachytherapy.* 2012;11:163–175.
28. Wehrmann C, Senftleben S, Zachert C, Muller D, Baum RP. Results of individual patient dosimetry in peptide receptor radionuclide therapy with ^{177}Lu DOTA-TATE and ^{177}Lu DOTA-NOC. *Cancer Biother Radiopharm.* 2007;22: 406–416.